Archives of Acoustics Vol. ***, No. ***, https://doi.org/10.24423/archacoust.2026.4407

Online First May 27, 2026

Research Paper

A Study of Damage Mode Recognition of Polypropylene Fiber-Reinforced Recycled Aggregate Concrete Based on Principal Components of Acoustic Emission Signals

Qianxu Chen[(1)], Xin Yang[(2)*]

[(1)] *James Watt School of Engineering, University of Glasgow*
Glasgow, United Kingdom

[(2)] *Institute of Marine and Environmental Geotechnical Engineering, Fujian University of Technology*
Fuzhou, China

*Corresponding Author: yangxin546@163.com

Received January 4, 2026; revised March 19, 2026; accepted March 20, 2026; available online March 25, 2026; version of record May 27, 2026; published issue XXXX.

To investigate the principal components of acoustic emission (AE) signals and the damage modes of polypropylene fiber (PPF)-reinforced recycled concrete, ten groups of specimens with coarse aggregate (CA) replacement rates of 0 % and 25 % and with different particle sizes, are designed and fabricated. Uniaxial compression AE tests are conducted to obtain AE parameters during the fracture process of PPF-reinforced recycled concrete. In this study, the Pearson correlation coefficient is employed to investigate the correlations among AE parameters. Then, principal component analysis (PCA) is performed on the AE signals to conduct dimensionality reduction of the multi-dimensional data. On this basis, the optimal number of clusters for the principal components of AE signals is determined based on the silhouette coefficient. Finally, the k-means clustering algorithm is introduced to perform cluster analysis on the principal components of AE signals of PPF-reinforced recycled concrete. The clustering results are compared with each other to explore the characteristics of each cluster and to identify the corresponding damage mode for each cluster. The discriminability of AE parameters with respect to damage modes is also investigated. The research findings can provide a reference for predicting the fracture mechanism of PPF-reinforced recycled concrete.

Keywords: polypropylene fiber (PPF)-reinforced recycled concrete, acoustic emission, Pearson correlation coefficient, principal component analysis, k-means clustering.

1. Introduction

At present, the factors restricting the widespread application of recycled concrete lie in the fact that its mechanical properties, such as compressive strength and tensile strength, are inferior to those of natural concrete. To address this problem, methods such as the addition of external fibers can be adopted. Adding polypropylene fiber (PPF) to recycled concrete is a relatively common method (Wang *et al.*, 2022).

In recent years, numerous scholars have investigated the characteristics of acoustic emission (AE) signals in fiber-reinforced concrete, including principal component analysis (PCA) (Tayfur *et al.*, 2018), digital image technology (Ashraf, Rucka, 2024; Sagar *et al.*, 2025), the b-value method (Ashraf, Rucka, 2023), 3D printing technology (Ingle, Prem, 2025), shear models (Kantekin, Bakir, 2025), fatigue behavior (Džolan *et al.*, 2024), three-point bending test (Umar *et al.*, 2023), and durability (Chkhachirou *et al.*, 2025). Zheng *et al.* (2022) distinguished two types of acoustic events, matrix cracking and steel fiber vibration, according to AE

technique. Zaki *et al.* (2023) utilized rise time/amplitude analysis to classify the damage modes. Kouta *et al.* (2021) found that both AE activity and fracture energy increase with the rise in fiber content and fiber length. Saha and Sagar (2021) classified the AE signals generated by fiber-reinforced concrete into two categories via machine learning methods: cement matrix cracking and fiber pull-out, and pointed out that the classification of AE waveforms might facilitate the understanding of damage evolution during the fracture process.

In the current paper, AE parameters are obtained by conducting AE monitoring tests on PPF-reinforced recycled concrete. Based on methods including the Pearson correlation coefficient, PCA, and k-means clustering, an analysis is conducted on the principal components of the AE parameters and the corresponding damage modes of PPF-reinforced recycled concrete. The research findings can provide a reference for predicting the fracture mechanism of PPF-reinforced recycled concrete.

2. Experimental details

2.1. Sample preparation

The PPFs employed in this experiment were manufactured by Shandong Runlin Wood Industry Co., Ltd., and their main properties are presented in Table 1.

Table 1. Physical and mechanical parameters of PPFs.

Fiber type	Diameter [mm]	Length [mm]	Tensile strength [MPa]	Fracture strength [MPa]	Elongation at break [%]	Initial modulus [GPa]	Density [g/cm^3]	Recommended dosage [kg/m^3]
Micro-PPF	0.036	19	≥450	450	17	4.8	0.91	0.9
Macro-PPF1	0.9	30	≥550	500	24	6.6	0.91	6.0
Macro-PPF2	0.9	50	≥550	500	24	6.6	0.91	6.0

In this experiment, ordinary Portland cement is used as the cementitious material, while medium sand from Zone II is adopted as the fine aggregate, with a particle size range of 0.15 mm to 4.75 mm. The particle size range of the coarse aggregate (CA) is 5 mm to 20 mm. The recycled CA is derived from waste C30 concrete, which is subjected to impurity removal, crushing, and subsequent sieving to obtain the recycled CA meeting the experimental requirements, as illustrated in Fig. 1.

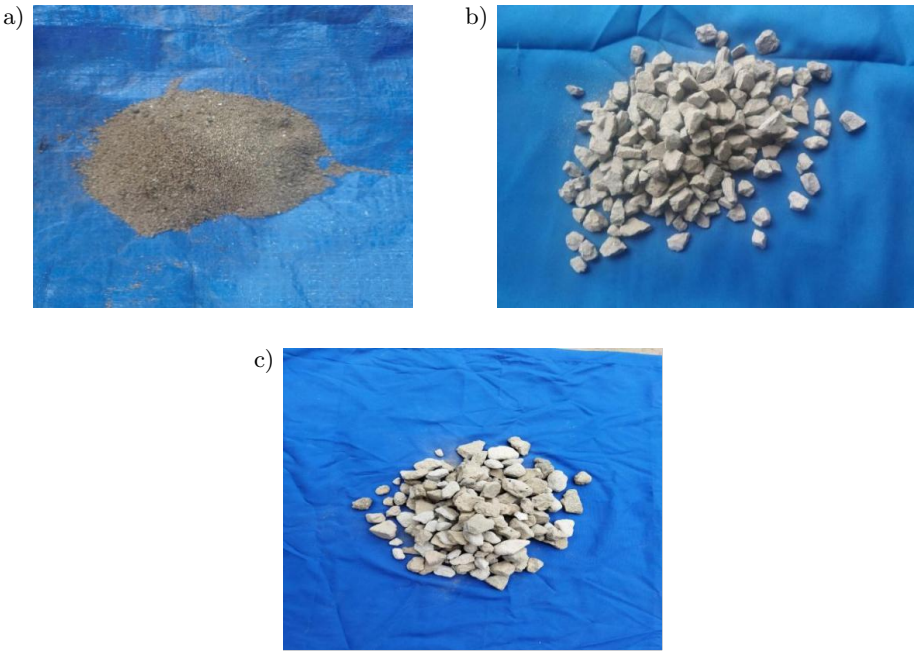

Fig. 1. Fine aggregate (a), natural coarse aggregate (b), and recycled coarse aggregate (c).

The concrete is prepared with a strength grade of C30, with a total of ten groups of specimens fabricated. The mix proportions are as follows: 358 kg/m^3 of cement, 706.15 kg/m^3 of medium sand, 1120.85 kg/m^3 of CA, and 215 kg/m^3 of water. The water-cement ratio is kept constant at 0.6 for all groups of specimens, while the variables are the CA replacement rate and fiber content. Specifically, the replacement rates of recycled CA are set at 0 % and 25 %, labeled as R-0 and R-25, respectively. In this experiment, both natural CA and recycled CA have a particle size range of 5 mm to 20 mm, with the proportion of the 5 mm to 10 mm fraction to the 10 mm to 20 mm fraction being 1:1. Specimen R-X-1 is a plain concrete specimen with no PPF added. Specimen R-X-2 incorporates microfibers at a dosage of 0.9 kg/m^3, while specimen R-X-3 incorporates macrofibers at a dosage of 6 kg/m^3. In addition, specimens R-X-4 and R-X-5 incorporate a hybrid blend of macrofibers and microfibers, with the total fiber dosage maintained at 6 kg/m^3. The specific mix proportions are provided in Table 2. Each group tested once for PCA.

Table 2. Mix proportions and properties of their test specimens.

Specimen no.	CA [kg/m^3]		Fiber length and fiber diameter [mm]	Fiber dosage [kg/m^3]	Compressive strength [MPa]
	Natural 5–10 / 10–20 [mm]	Recycled 5–10 / 10–20 [mm]			
Zero CA substitution					
R-0-1	560/560	0	None	0	37.68
R-0-2	560/560	0	19/0.036	0.9	38.99
R-0-3	560/560	0	50/0.9	6	45.94
R-0-4	560/560	0	19/0.036+30/0.9	0.9+5.1	42.92
R-0-5	560/560	0	19/0.036+50/0.9	0.9+5.1	41.13
25 % CA substitution					
R-25-1	420/420	140/140	None	0	33.23
R-25-2	420/420	140/140	19/0.036	0.9	35.56
R-25-3	420/420	140/140	50/0.9	6	44.09
R-25-4	420/420	140/140	19/0.036+30/0.9	0.9+5.1	43.46
R-25-5	420/420	140/140	19/0.036+50/0.9	0.9+5.1	51.75

2.2. Tests

In accordance with the requirements of Ministry of Housing and Urban-Rural Development of the PRC (2019), cube specimens with a side length of 150 mm are prepared. After the concrete mixture is poured into the molds, the specimens are cured at room temperature for one day. Subsequently, the specimens are demolded, labeled, and then subjected to natural curing in a curing room for 28 days. An HCT306B compression testing machine (Fig. 2) is employed for the uniaxial compression test, with a loading rate of 0.5 MPa/s. An AMSY-6 AE testing

Fig. 2. HCT306B compression testing machine.

system is adopted for AE monitoring, and the threshold of the AE instrument is set at 40 dB, with a sampling frequency of 5 MHz, to minimize the impact of ambient noise during the test.

3. Damage mode identification based on AE parameters

3.1. Preliminary screening of AE parameters based on the Pearson correlation coefficient method

The Pearson correlation coefficient can reflect the degree of linear correlation between two variables; its value ranges from −1 to 1, with a larger absolute value indicating a stronger correlation. Therefore, the Pearson correlation coefficient method can be adopted for the preliminary screening of AE characteristic parameters, with the aim of selecting parameters with low correlation coefficients and high mutual independence as far as possible, thereby reducing the size of the characteristic parameter set. Equation (1) presents the calculation formula for the Pearson correlation coefficient r. When $r = 1$, it indicates a perfect positive linear correlation between the two variables, when $r = -1$, it indicates a perfect negative linear correlation, and when $r = 0$, it indicates no linear correlation between them:

$$r = \frac{\sum_{i=1}^{n}(x_i - \overline{x})(y_i - \overline{y})}{\sqrt{\sum_{i=1}^{n}(x_i - \overline{x})^2 \sum_{i=1}^{n}(y_i - \overline{y})^2}}, \tag{1}$$

where x_i and y_i represent the i-th observed values of the two variables x and y, respectively, $\overline{x}$ and $\overline{y}$ denote the sample means of variables x and y, and n is the sample size.

In this paper, six AE characteristic parameters, namely amplitude, rise time, duration, count, energy, and dominant frequency, were selected for the Pearson correlation coefficient analysis. These parameters characterize the AE signals in multiple aspects in both the time and frequency domains, and are thus capable of comprehensively reflecting the AE behavior during the damage process.

Table 3 presents the Pearson correlation coefficients among the six AE characteristic parameters, namely amplitude, rise time, duration, count, energy, and dominant frequency. Based on the values of the correlation coefficients, parameters with a coefficient greater than 0.6 were regarded as having a strong correlation, in which case one of the characteristic parameters could be discarded. As can be seen from Table 3, the Pearson correlation coefficients between the three parameters (rise time, energy, and dominant frequency) and the other parameters are mostly less than 0.6, indicating low correlation and high independence of these three parameters. The Pearson correlation coefficients among the three parameter pairs – amplitude and count, amplitude and duration, and count and duration – are mostly greater than 0.6, indicating a strong correlation between each pair. Among these parameters, amplitude and count have well-defined physical meanings: the higher their values, the stronger the acoustic emission activity. In contrast, duration generally needs to be interpreted comprehensively in combination with other parameters. Therefore, five AE characteristic parameters, namely amplitude, rise time, count, energy and dominant frequency, were selected for PCA.

3.2. Selection of characteristic parameters based on PCA

PCA is a data dimensionality reduction method that transforms standardized parameter data into several uncorrelated principal component variables via dimensionality reduction, thus capturing most of the information contained in the original dataset. To eliminate the influence of dimensional differences among different characteristic parameters, the data need to be standardized prior to performing PCA.

Assuming that the original dataset is denoted as X, it is then subjected to standardization to yield the sample matrix X_{n*p}, where n is the number of samples and p is the number of features. The covariance matrix R_{p*p} is

Table 3. Pearson correlation coefficients between different AE parameters.

Specimen no.	AE parameter	Amplitude	Rise time	Duration	Count	Energy
R-0-1	Rise time	0.43	–	–	–	–
	Duration	0.75	0.63	–	–	–
	Count	0.87	0.5	0.84	–	–
	Energy	0.53	0.13	0.26	0.51	–
	Dominant frequency	0.17	0.1	0.16	0.22	0.1
R-0-2	Rise time	0.63	–	–	–	–
	Duration	0.84	0.75	–	–	–
	Count	0.87	0.7	0.94	–	–
	Energy	0.55	0.31	0.39	0.51	–
	Dominant frequency	−0.05	−0.1	−0.11	−0.02	0.03
R-0-3	Rise time	0.19	–	–	–	–
	Duration	0.57	0.36	–	–	–
	Count	0.71	0.27	0.75	–	–
	Energy	0.5	−0.01	0.13	0.37	–
	Dominant frequency	0.21	0.03	0.14	0.29	0.1
R-0-4	Rise time	0.06	–	–	–	–
	Duration	0.4	0.21	–	–	–
	Count	0.49	0.08	0.58	–	–
	Energy	0.38	−0.03	0.05	0.23	–
	Dominant frequency	−0.01	−0.01	0.1	0.27	−0.03
R-0-5	Rise time	0.08	–	–	–	–
	Duration	0.34	0.17	–	–	–
	Count	0.77	0.09	0.38	–	–
	Energy	0.32	0.02	0.05	0.15	–
	Dominant frequency	0.31	0.01	0.06	0.51	0.02
R-25-1	Rise time	0.03	–	–	–	–
	Duration	0.17	0.09	–	–	–
	Count	0.58	0.02	0.3	–	–
	Energy	0.66	0.02	0.04	0.51	–
	Dominant frequency	0.08	−0.05	0.06	0.27	0.07
R-25-2	Rise time	0.04	–	–	–	–
	Duration	0.42	0.18	–	–	–
	Count	0.49	0.07	0.6	–	–
	Energy	0.48	−0.02	0.07	0.17	–
	Dominant frequency	0.01	0.002	0.07	0.22	−0.06
R-25-3	Rise time	0.35				
	Duration	0.67	0.49	–	–	–
	Count	0.75	0.41	0.83	–	–
	Energy	0.47	0.08	0.19	0.42	–
	Dominant frequency	0.005	0.01	−0.02	−0.01	0.07
R-25-4	Rise time	0.11	–	–	–	–
	Duration	0.47	0.21	–	–	–
	Count	0.48	0.11	0.64	–	–
	Energy	0.49	0.001	0.09	0.11	–
	Dominant frequency	−0.09	−0.1	0.02	0.1	−0.17
R-25-5	Rise time	0.52	–	–	–	–
	Duration	0.78	0.69	–	–	–
	Count	0.8	0.65	0.93	–	–
	Energy	0.47	0.21	0.29	0.45	–
	Dominant frequency	−0.13	−0.12	−0.18	−0.13	−0.03

calculated according to Eq. (2). The covariance matrix is then subjected to eigenvalue decomposition to derive p eigenvalues, which are then sorted in descending order to obtain $\lambda_1, \lambda_2, ..., \lambda_p$ and their corresponding

$T_1, T_2, ..., T_p$. At this point, the i-th calculated principal component can be expressed by Eq. (3), while the contribution rate of the principal component ϕ_k can be expressed by Eq. (4):

$$R_{p*p} = \frac{1}{n-1} X^T_{n*p} X_{n*p}, \tag{2}$$

$$\mathrm{PCA}(i) = T_{1i}X_1 + T_{2i}X_2 + \cdots + T_{pi}X_p, \tag{3}$$

$$\phi_k = \frac{\lambda_k}{\sum_{i=1}^{p} \lambda_i}, \tag{4}$$

where ϕ_k denotes the contribution rate of the k-th principal component.

Based on the results of the Pearson correlation coefficient analysis, five characteristic parameters, namely amplitude, rise time, count, energy, and dominant frequency, were selected for PCA. Table 4 presents the contribution rates of each principal component for the specimens. As can be seen from Table 4, the cumulative contribution rate of the first three principal components exceeds 75 %, indicating that the selection of these three principal components can well retain most of the information from the original dataset.

Table 4. Contribution rates of each principal component and the cumulative contribution rate of the first three principal components (PCs) [%].

Specimen no.	1	2	3	4	5	Cumulative contribution of PCs 1:3
R-0-2	56.4	20.4	13.7	6.9	2.6	90.5
R-0-3	44.7	20.5	18.5	10.9	5.4	83.7
R-0-4	35.4	22.2	20.2	13.6	8.6	77.8
R-0-5	48.8	20.5	16.6	11.1	3	85.9
R-25-2	35.9	22.7	20	13.8	7.6	78.6
R-25-3	46.2	20.4	18.2	10.4	4.8	84.8
R-25-4	35.7	23.1	19.5	14.5	7.2	78.3
R-25-5	52.6	19.8	15.8	8.3	3.5	88.2

3.3. Determination of the optimal number of clusters

In the process of conducting cluster analysis, determining a reasonable number of clusters is a key step in ensuring the reliability of the results. An excessively small number of clusters may result in different damage modes being incorrectly classified into the same category. Conversely, an excessively large number of clusters may lead to the over-segmentation of the same damage mode. In this paper, the silhouette coefficient is adopted to evaluate the number of clusters. The range of the number of clusters was initially set to 2–6, and the silhouette coefficient was used to evaluate the performance of each cluster number, thereby determining the optimal number of clusters ultimately.

The silhouette coefficient (SI) is an index that calculates two metrics: the average distance between a sample and other samples within its own cluster, and the average distance between the sample and the samples within the nearest neighboring cluster. It evaluates the compactness and separation of clustering by measuring the difference between these two distances. A larger SI indicates more reasonable sample clustering and higher clustering quality. The calculation equation for the SI is given by

$$\mathrm{SI} = \frac{b(i) - a(i)}{\max\{a(i), b(i)\}}, \tag{5}$$

where $a(i)$ and $b(i)$ denote the average distance from sample i to other samples within the same cluster and to all samples in the nearest neighboring cluster, respectively.

Figure 3 presents the number of clusters calculated based on the SI index. It can be seen that the SI index reaches its maximum value when the number of clusters is set to 4; therefore, the optimal number of clusters is determined to be 4.

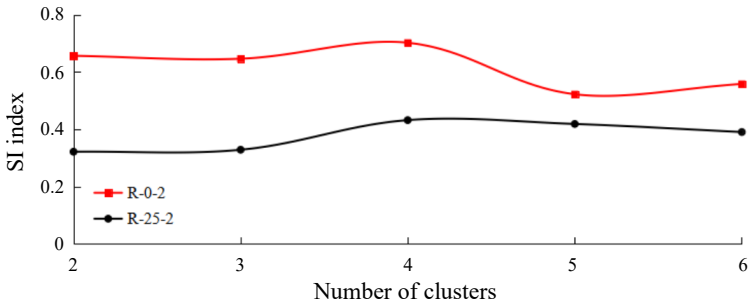

FIG. 3. Number of clusters assessed by the SI index.

4. Analysis of clustering results

In this paper, the k-means clustering algorithm was adopted to perform cluster analysis on the results of principal component analysis of AE parameters of PPF-reinforced recycled concrete, and the number of clusters was set to 4, as determined in Subsec. 3.3.

4.1. k-means clustering

k-means is an iterative clustering algorithm whose operating principle can be outlined as follows: given a sample dataset composed of n samples $X_1, X_2, ..., X_n$, the algorithm aims to partition these samples into k-distinct clusters. Here, m_i the centroid (mean vector) of the samples assigned to the i-th cluster. The algorithm employs the distanceas the distance metric. The detailed steps are as follows (Wen, 2025):

1. Initialization: randomly and uniformly select k observation samples as the initial cluster centers m_1–m_k.
2. Assignment: assign each sample data point to the cluster whose center is nearest to it, based on the Euclidean distance.
3. Update: recalculate the mean vector (cluster center) for each cluster based on the sample data points assigned to it.
4. Iteration: repeat steps (2) and (3) until one of the following conditions is met: the predefined maximum number of iterations is reached, or the cluster centers no longer change (i.e., the mean vectors converge). Once these conditions are satisfied, the model is considered built, and the final clustering results are output.

4.2. Clustering results

Table 5 presents the characteristic ranges of the four clusters calculated by the k-means algorithm. Among these clusters, cluster 1 is characterized by low amplitude (below 90 dB) and low energy, cluster 2 features low dominant frequency (below 40 kHz) and high rise time, cluster 3 is defined by high dominant frequency (above 100 kHz), relatively high amplitude (around 90 dB), and relatively high energy, and cluster 4 exhibits high amplitude (close to 100 dB) and high energy.

4.3. Damage mode identification

Bian *et al.* (2021) classified the damage modes of fiber-reinforced concrete into three categories: matrix cracking, fiber-matrix debonding, and fiber pull-out. Based on the findings presented in Subsec. 4.2, cluster 1 is characterized by low amplitude (below 90 dB) and low energy, corresponding to matrix cracking failure. Cluster 3 is characterized by high dominant frequency (above 100 kHz), relatively high amplitude (around 90 dB), and relatively high energy, corresponding to fiber-matrix debonding failure. Cluster 4 is characterized by high amplitude (close to 100 dB) and high energy, corresponding to fiber pull-out failure. Cluster 2, by contrast, is characterized by low dominant frequency (below 40 kHz) and high rise time, corresponding to mechanical noise.

As can be seen from Table 5, the AE characteristic parameters exhibit different performance levels. Both amplitude and energy can be used to distinguish the three different damage modes, namely matrix cracking, fiber-matrix debonding, and fiber pull-out; however, relatively speaking, energy demonstrates better discrimination

Table 5. Range of clustering features (the average value is given in square brackets).

Specimen no.	AE parameter	Cluster 1	Cluster 2	Cluster 3	Cluster 4
R-0-2	Amplitude [dB]	60.1–89.6 [68.8]	69.2–100 [87.8]	70.5–100 [90.8]	99.9–100 [99.9]
	Rise time [ms]	0.01–42.5 [4.9]	0.2–104.9 [52.5]	1.1–103.8 [48.1]	0.7–104.2 [45.2]
	Count	11–5715 [4860]	1435–9182[5629]	1685–9019 [6869]	6049–8956 [7867]
	Energy [10^6 aJ]	0.001–3.6 [0.1]	0.2–80.3 [12.8]	0.3–77.1 [20]	88.5–394 [152.4]
	Dominant frequency [kHz]	26.2–125.1 [61.5]	26.9–68.4 [35.1]	59.8–123.3 [108]	27.5–109.2 [69.9]
R-0-3	Amplitude [dB]	60.1–92.4 [77.6]	72.9–100 [88.8]	76.8–100 [89.5]	92.3–100 [99]
	Rise time [ms]	0.003–69.5 [16.5]	1.1–104.8 [63.2]	0.2–104.8 [53.8]	0.6–101.3 [42.1]
	Count	21–6523 [3324]	3476–8728 [6031]	1898–9608 [6467]	4783–9706 [7795]
	Energy [10^6 aJ]	0.008–9.7 [1.3]	0.5–46.4 [9.4]	0.8–53.9 [10.2]	13.4–467 [86.4]
	Dominant frequency [kHz]	26.2–120.2 [37.9]	28.1–72 [36.2]	62.9–123.9 [106.9]	28.1–122.7 [65.2]
R-0-4	Amplitude [dB]	60.4–100 [87.6]	81.2–100 [93.2]	79–100 [90.4]	94.5–100 [99.6]
	Rise time [ms]	0.1–101.9 [30.5]	36.3–104.8 [79.2]	0.02–104.7 [53.5]	0.1–103.2 [37.5]
	Count	64–7861 [5386]	2989–8682 [6575]	4127–8717 [6875]	5454–10023 [7946]
	Energy [10^6 aJ]	0.006–32.5 [11.9]	1.8–171 [26.8]	1.1–74.8 [14]	11.6–1910 [142.3]
	Dominant frequency [kHz]	28.1–116.6 [34.5]	25.6–90.9 [34.4]	56.2–123.9 [109.9]	28.1–116.6 [65.7]
R-0-5	Amplitude [dB]	60.2–99 [73.2]	71–100 [89.9]	69.8–100 [91.4]	99.1–100 [100]
	Rise time [ms]	0.01–52 [12.4]	0.008–104.4 [52.2]	1.3–104 [52.1]	1.9–103.4 [47.8]
	Count	92–5249 [1371]	1643–9068 [5991]	1256–8968 [6803]	6109–8949 [7801]
	Energy [10^6 aJ]	0.004–18.7 [0.5]	0.2–236 [30.2]	0.2–377 [38.5]	133–2600 [522]
	Dominant frequency [kHz]	28.7–166 [56.1]	28.7–76.9 [35]	62.3–128.5 [106.7]	28.7–110.5 [52.6]
R-25-2	Amplitude [dB]	60.4–99.2 [85.2]	85.1–100 [95.4]	77.3–100 [91.1]	86.7–100 [96.7]
	Rise time [ms]	0.03–104.3 [48.4]	49.1–104.6 [79.4]	0.2–104.8 [50.3]	0.1–84.9 [25.9]
	Count	84–7954 [5562]	4128–8587 [6901]	4775–8733 [6942]	4294–8714 [6912]
	Energy [10^6 aJ]	0.005–43.6 [6.2]	2.2–218 [43.2]	1.4–113 [15.9]	4.5–1030 [66.4]
	Dominant frequency [kHz]	26.2–113.5 [35.1]	26.2–115.4 [38.1]	59.2–161.1 [110.3]	26.9–114.7 [37.1]
R-25-3	Amplitude [dB]	60.1–94.7 [74.2]	75.8–100 [89.4]	70.6–100 [88.3]	95.1–100 [99.7]
	Rise time [ms]	0.01–51.5 [10.5]	0.1–104.8 [52.1]	0.3–104.4 [54.3]	3.5–97.8 [42.6]
	Count	26–6190 [1718]	1927–9135 [6282]	2429–9091 [5954]	4474–9940 [8403]
	Energy [10^6 aJ]	0.002–7 [0.6]	0.5–109 [16.4]	0.3–78.4 [10.8]	55.1–607 [127.3]
	Dominant frequency [kHz]	27.5–121.5 [69.4]	26.9–68.4 [34.2]	69.6–125.1 [109.7]	28.1–128.1 [87.6]
R-25-4	Amplitude [dB]	62.1–97 [84.9]	80.5–100 [94.3]	80.3–100 [92.7]	91.4–100 [98.3]
	Rise time [ms]	0.05–87.7 [27.5]	36.1–104.8 [77.1]	0.3–104.2 [50.6]	0.3–100.6 [32.1]
	Count	74–7802 [5170]	4426–8673 [6617]	4952–8794 [6964]	4362–8842 [6988]
	Energy [10^6 aJ]	0.008–66.2 [5.9]	1.4–186 [30.1]	1.5–116 [16.3]	6.4–727 [107.2]
	Dominant frequency [kHz]	28.1–125.7 [47]	28.3–109.3 [37.3]	37.2–192.3 [111.5]	28.1–122.7 [38.5]
R-25-5	Amplitude [dB]	60–94.9 [72.7]	73.7–100 [88.2]	73.1–100 [89.1]	96.8–100 [99.9]
	Rise time [ms]	0.01–43.5 [8.4]	0.6–104.1 [49.8]	0.7–104.2 [51.6]	0.6–104.3 [47.6]
	Count	28–5326 [1050]	1349–9215 [5806]	1952–9253 [6322]	6074–9522 [8373]
	Energy [10^6 aJ]	0.002–9.5 [0.5]	0.3–217 [14.9]	0.3–192 [15.9]	163–968 [389]
	Dominant frequency [kHz]	29.9–123.9 [81.6]	28.1–60.4 [33.1]	75.1–123.2 [107.1]	28.1–115.4 [66.5]

performance. Taking specimen R-0-2 as an example, the average amplitude of fiber-matrix debonding is 1.32 times that of matrix cracking, and the average amplitude of fiber pull-out is 1.1 times that of fiber-matrix debonding. The average energy of fiber-matrix debonding is 200 times that of matrix cracking, and the average energy of fiber pull-out is 7.6 times that of fiber-matrix debonding. The dominant frequency can be used to distinguish mechanical noise. The average dominant frequency of mechanical noise is below 40 kHz, with most values of this cluster falling within the range of 28 dB to 80 dB, and only a few high-frequency events (above 100 dB). The count exhibits poor discrimination performance: matrix cracking failure is associated with a low count, while it is difficult to distinguish among the other three damage types using this parameter.

There is a certain correlation between compressive strength and matrix cracking. The lower the energy of matrix cracking, the higher the compressive strength of the specimen. Overall, the energy of specimens R-X-3 and R-X-5 is relatively low, while their compressive strength is relatively high.

5. Conclusions

This paper presented a study on the PCA of AE parameters and the damage modes of PPF-reinforced recycled concrete, and the following conclusions can be drawn:

1. The study showed that the Pearson correlation coefficients between the three parameters (rise time, energy, and dominant frequency) and the other parameters are mostly less than 0.6, indicating low correlation and high independence of these three parameters. The Pearson correlation coefficients among the three parameter pairs – amplitude and count, amplitude and duration, and count and duration – are mostly greater than 0.6, indicating a strong correlation between each pair. Five AE characteristic parameters, namely amplitude, rise time, count, energy, and dominant frequency, were selected for the PCA of PPF-reinforced recycled concrete.
2. Based on the SI index, the optimal number of clusters for the principal components of PPF-reinforced recycled concrete was determined to be 4. The unsupervised learning algorithm of k-means clustering was applied to identify the damage modes of PPF-reinforced recycled concrete, with four distinct damage modes being identified as follows:
   - mechanical noise, featuring low dominant frequency (below 40 kHz) and high rise time,
   - matrix cracking, characterized by low amplitude (below 90 dB) and low energy,
   - fiber-matrix debonding, exhibiting high dominant frequency (above 100 kHz), relatively high amplitude (around 90 dB) and relatively high energy,
   - fiber pull-out, characterized by high amplitude (close to 100 dB) and high energy.
3. The AE characteristic parameters exhibit varying discrimination performance. Both amplitude and energy can be used to distinguish the three distinct damage modes, namely matrix cracking, fiber-matrix debonding, and fiber pull-out; however, energy demonstrates superior discrimination performance. The dominant frequency can be used to distinguish mechanical noise, whereas the count exhibits poor discrimination performance.

It should be pointed out that some conclusions of this study need to be further verified by fiber pull-out tests.

Fundings

This study was supported by the Fujian Natural Science Foundation (Grant no. 2022J01930), the authors gratefully acknowledge this support.

Conflict of interests

The authors declare that there are no known competing financial interests or personal relationships that could have influenced the work described in this paper.

Authors' contributions

Qianxu Chen performed the analysis and contributed to data interpretation. Xin Yang conceptualized the study and wrote the original draft. All authors reviewed and approved the final manuscript.

References

1. Ashraf S., Rucka M. (2023), Microcrack monitoring and fracture evolution of polyolefin and steel fibre concrete beams using integrated acoustic emission and digital image correlation techniques, *Construction and Building Materials*, **395**: 132306, https://doi.org/10.1016/j.conbuildmat.2023.132306.

2. Ashraf S., Rucka M. (2024), Comparative study on fracture evolution in steel fibre and bar reinforced concrete beams using acoustic emission and digital image correlation techniques, *Case Studies in Construction Materials*, **20**: e03359, https://doi.org/10.1016/j.cscm.2024.e03359.
3. Bian C., Wang J.Y., Guo J.Y. (2021), Damage mechanism of ultra-high performance fibre reinforced concrete at different stages of direct tensile test based on acoustic emission analysis, *Construction and Building Materials*, **267**: 120927, https://doi.org/10.1016/j.conbuildmat.2020.120927.
4. Chkhachirou M., El-Hassan H., El-Maaddawy T. (2025), Durability of BFRP bars embedded in geopolymer concrete under hygrothermal exposure and sustained loading, *Case Studies in Construction Materials*, **23**: e05571, https://doi.org/10.1016/j.cscm.2025.e05571.
5. Džolan A., Fischer O., Niedermeier R. (2024), Analyses of the fatigue behavior of carbon short-fiber-reinforced concrete (CSFRC) under tension and flexion, *Construction and Building Materials*, **453**: 139058, https://doi.org/10.1016/j.conbuildmat.2024.139058.
6. Ingle V.V., Prem P.R. (2025), Acoustic emission examination of 3D printed ultra-high performance concrete with and without coarse aggregate under fresh and hardened states, *Journal of Building Engineering*, **111**: 113491, https://doi.org/10.1016/j.jobe.2025.113491.
7. Kantekin Y., Bakir B.B. (2025), Joint shear model for fiber reinforced concrete beam-column connections, *Journal of Building Engineering*, **101**: 111833, https://doi.org/10.1016/j.jobe.2025.111833.
8. Kouta N., Saliba J., Saiyouri N. (2021), Fracture behavior of flax fibers reinforced earth concrete, Engineering Fracture Mechanics, **241**: 107378, https://doi.org/10.1016/j.engfracmech.2020.107378.
9. Ministry of Housing and Urban-Rural Development of the PRC (2019), *Standard for test methods of concrete physical and mechanical properties* (Standard No. GB/T 50081-2019).
10. Sagar R.V., Samadhan S.A., Kundu T. (2025), Tensile stress-crack width relationship for steel fiber reinforced concrete under mode I fracture, *Mechanics Research Communications*, **144**: 104378, https://doi.org/10.1016/j.mechrescom.2025.104378.
11. Saha I., Sagar R.V. (2021), Classification of the acoustic emissions generated during the tensile fracture process in steel fibre reinforced concrete using a waveform-based clustering method, *Construction and Building Materials*, **294**: 123541, https://doi.org/10.1016/j.conbuildmat.2021.123541.
12. Tayfur S., Alver N., Adbi S., Saatci S., Ghiami A. (2018), Characterization of concrete matrix/steel fiber debonding in an SFRC beam: Principal component analysis and k-mean algorithm for clustering AE data, *Engineering Fracture Mechanics*, **194**: 73–85, https://doi.org/10.1016/j.engfracmech.2018.03.007.
13. Umar H.A., Zeng X.H., Long G.C., Tang Z., Lan X.L., Zhu H.S. (2023), Synergistic effects of asphalt emulsion and fiber reinforcement on fracture properties and energy absorption of self-compacting concrete, *Theoretical and Applied Fracture Mechanics*, **127**: 104043, https://doi.org/10.1016/j.tafmec.2023.104043.
14. Wang C.Q., Zhang Y.Y., Ma Z.M., Wang D.J. (2022), Hysteretic deteriorating behaviors of fiber-reinforced recycled aggregate concrete composites subjected to cyclic compressive loadings, *Journal of Building Engineering*, **49**: 104087, https://doi.org/10.1016/j.jobe.2022.104087.
15. Wen Y.J. (2025), *Research on damage pattern identification and evolution mechanism of steel-concrete structures based on acoustic emission and machine learning* [in Chinese], M.Sc. Thesis, Guangxi University.
16. Zaki Y.A., Abouhussien A.A., Hassan A.A.A., Ismail M.K., AbdelAleem B.H. (2023), Crack detection and classification of repaired concrete beams by acoustic emission monitoring, *Ultrasonics*, **134**(5): 107068, https://doi.org/10.1016/j.ultras.2023.107068.
17. Zheng Q.M., Li C., He B., Jiang Z.W. (2022), Revealing the effect of silica fume on the flexural behavior of ultra-high-performance fiber-reinforced concrete by acoustic emission technique, *Cement and Concrete Composites*, **131**(6): 104563, https://doi.org/10.1016/j.cemconcomp.2022.104563.